Available online at www.sciencedirect.com
SCIENCE DIRECT®
Journal of Power Sources 141 (2005) 65–78
JOURNAL OF POWER SOURCES
www.elsevier.com/locate/jpowsour

CFD-based modelling of proton exchange membrane fuel cells

B.R. Sivertsen[a,1], N. Djilali[b,*]

[a] *Norwegian University of Science and Technology, NTNU, Norway*
[b] *Institute for Integrated Energy Systems, University of Victoria, Vic., BC, Canada V8W 3P6*

Received 28 July 2004; accepted 31 August 2004
Available online 6 November 2004

Abstract

A comprehensive non-isothermal, 3D computational model for proton exchange membrane (PEM) fuel cells has been developed, and implemented into a computational fluid dynamic (CFD) code. The model allows parallel computing, thus making it practical to perform well-resolved simulations for large computational domains. The model accounts for convective and diffusive transport and allows prediction of the concentration of species. Distributed heat generation associated with the electrochemical reaction in the cathode and anode is included in the model. The model solves for the electric and ionic potentials in the electrodes and membrane, and the local activation overpotential distribution is resolved, rather than assumed uniform, making it possible to predict the local current density distribution more accurately.

Maximum current densities are predicted under the land areas as a result of the dominant influence of ohmic losses over concentration losses on the activity at the catalyst layer. A parametric analysis shows that substantially different spatial distributions can be obtained by varying the asymmetry parameter with no noticeable change in the global current density and polarization curve. Changing the conductivity radically alters the current distribution by changing the relative influence of ohmic to activation overpotentials.

Keywords: PEM fuel cell; Fuel cell modeling; Overpotential; Simulation; CFD; Parallel computing

1. Introduction

Recent years have seen significant increase in power densities, reliability and overall performance of proton exchange membrane (PEM) fuel cells, but the underlying physics of the transport processes in a fuel cell— which involve coupled fluid flow, heat and mass transport with electrochemistry— remain poorly understood. The development of physically representative models that allow reliable simulation of the processes under realistic conditions is essential to the development and optimization of fuel cells, the introduction of cheaper materials and fabrication techniques, and the design and development of novel architectures.

The difficult experimental environment of fuel cell systems has stimulated efforts to develop model that could simulate and predict multi-dimensional coupled transport of reactants, heat and charged species using computational fluid dynamic (CFD) methods. The first applications of CFD methods to fuel cells focused on two-dimensional models ([1–4]). More recently, CFD and improved transport models have allowed the development of increasingly more realistic computational models, accounting for fluid, thermal and electrochemical transport, complex three-dimensional geometries including flow and cooling channels, and two-phase transport (e.g. [5–8]).

Simulations of 3D PEMFC geometries have required some simplifications in order to reduce computational requirements. In particular, it is only very recently that CFD-based models have started to include resolved catalyst layers and to account for non-uniform distributions of overpotentials at the electrodes [9–11]. A common issue to many computational models is the uncertainties associated with the specification of various parameters that impact the transport processes. As-

* Corresponding author. Tel.: +1 250 721 6034; fax: +1 250 721 6323.
E-mail addresses: ndjilali@uvic.ca (N. Djilali); brsi@statoil.com (B.R. Sivertsen)
[1] Present address: Statoil ASA, Corporate Strategic Technology, Trondheim, Norway.

0378-7753/$ – see front matter © 2004 Elsevier B.V. All rights reserved.
doi:10.1016/j.jpowsour.2004.08.054

sessing the sensitivity of the flow, thermal or electrochemical response to these uncertainties is essential.

In this paper a single-phase, three-dimensional, non-isothermal model is presented. This model is implemented into the commercial CFD code Fluent 6.1, with custom-developed user-subroutines that take account of the physico-chemical processes associated with PEM fuel cells. The model has the capability of resolving the catalyst layer, and, in contrast with most published models, this model accounts for a distributed overpotential at the cathodic catalyst layer, and heat sources at each electrode, rather than lumping the heat sources/sinks at the cathode as is common practice. This model also takes into account convection and diffusion of different species in the channels as well as in the porous gas diffusion layer, heat transfer in the solids as well as in the gases, electrochemical reactions and the transport of liquid water through the membrane. Large scale and fine mesh simulations for fuel cells remain relatively scarce due to the computer intensive nature of the numerical models. A key feature of the model implementation presented here is parallel computing which allows simulations with finer mesh resolution and/or a large number of computational nodes.

2. Model description and field equations

The model presented here is a full three-dimensional model that resolves coupled transport processes in the membrane, catalyst layer, gas diffusion electrodes and reactant flow channels of a PEM fuel cell. The model was implemented via a set of user defined subroutines in a commercial CFD code, Fluent 6.1 [12]. The implementation allows simulations using parallel processing. The assumptions and governing equations are presented in this section.

2.1. Assumptions

Under constant load conditions, a fuel cell is assumed to operates in steady state. Since the gas streams in the flow channels are humidified, hydrogen and air at low velocities (Reynolds number), laminar flow and ideal gas behaviour are assumed. The complex nature of the transport processes in PEM fuel cells precludes systematic modelling of all processes in a three-dimensional model, and phenomena that are second order under normal operating conditions are neglected:

- All water produced in the electrochemical reactions is assumed to be in the gas phase, and phase change and two phase-transport are not considered.
- Dilute solution theory is used to determine the species diffusion.
- The membrane is assumed to be fully humidified and its protonic conductivity is taken to be constant.
- The membrane is considered impermeable to gases and cross-over of reactant gases is neglected [13].
- Ohmic heating in the bipolar plates and in the gas diffusion electrodes is neglected due to high conductivity.
- Ohmic heating is neglected in the membrane. Heat transport in the membrane is assumed to take place due to conduction only.
- Electro-neutrality prevails inside the membrane. The proton concentration in the membrane is assumed to be constant and equal to the concentration of fixed sulfonic acid groups.
- The overpotential at the anode is assumed to be constant.
- The gas diffusion layer is assumed to be homogeneous and isotropic.

2.2. Model equations in gas flow channels

CFD codes are structured around numerical algorithms that solve equations representing physical conservation laws in order to obtain the velocity field and associated mass, heat and scalar transport quantities. The three-dimensional steady state mass conservation (continuity) equation is given by:

$$\frac{\partial(\rho u)}{\partial x} + \frac{\partial(\rho v)}{\partial y} + \frac{\partial(\rho w)}{\partial z} = 0 \tag{1}$$

where ρ is the density of the mixture, and u, v and w are the velocities in the x, y and z direction, respectively. The density of the mixture is calculated using:

$$\rho = \frac{1}{\sum_i y_i/\rho_i} \tag{2}$$

where y_i is the mass fraction of species i. The density of each species, ρ_i is obtained from the perfect gas law relation:

$$\rho_i = \frac{p_{op} M_i}{RT} \tag{3}$$

in which p_{op} corresponds to the anode or cathode side pressure, M_i is the molecular weight, T is the temperature and R is the universal gas constant.

The flow field is governed by the steady state Navier–Stokes equations, which express momentum conservation for a Newtonian fluid. A convenient formulation for CFD is:

$$\nabla \cdot (\rho \mathbf{v}\mathbf{v}) = -\nabla \mathbf{p} + \nabla \tau + S_{\text{mom}} \tag{4}$$

where $\mathbf{v}$ and $\mathbf{p}$ are the velocity and pressure vectors, τ is the viscous stress tensor matrix and S_{mom} is a momentum source.

2.2.1. Mass transport equations

The steady state mass transport equation can be written in the following general form:

$$\nabla \cdot (\rho \mathbf{v} y_i) = -\nabla \cdot \mathbf{j}_i + S_i \tag{5}$$

where y_i is the mass fraction of species i, $\mathbf{j}_i$ is the diffusive mass flux vector. The source term S_i is set to zero in the flow channels, where no reaction takes place. Multicomponent effects are usually considered to be small in dilute solutions and in solutions where the species are of similar size and

nature [14,15]. In order to account for the tortuosity in the porous media in the electrodes, the dilute diffusion model had to be used. In Fluent 6.1 there is no straight forward way of taking into account the tortuosity when the Maxwell–Stefan equations are applied.

The diffusive mass flux vector $\mathbf{j}_i$ can be written as [16]:

$$\mathbf{j}_i = -\sum_{j=1}^{N-1} \rho D_{ij} \nabla y_j \tag{6}$$

where D_{ij} is the binary-diffusion coefficient.

The binary diffusion coefficients are dependent on temperature and pressure. They can be calculated according to the empirical relation [14]:

$$D_{ij} = \frac{T^{1.75}(1/M_i + 1/M_j)^{1/2}}{p\left(\left(\sum_k V_{ki}\right)^{1/3} + \left(\sum_k V_{kj}\right)^{1/3}\right)^2} \times 10^{-3} \tag{7}$$

where D_{ij} is the binary diffusion coefficient, T is the temperature in Kelvin, p is the pressure in atm, M_i is the molecular weight of species i, and V_{ki} is the atomic diffusion volume. The values for $\sum V_{ki}$ is given by Cussler [14].

2.2.2. Energy transport

The energy equation, which expresses the first law of thermodynamics, can be expressed as:

$$\nabla \cdot (\mathbf{v}(\rho E + p)) = \nabla \left(k_{\text{eff}} \nabla T - \sum_j h_j \mathbf{j}_j + (\tau_{\text{eff}} \cdot \mathbf{v}) \right) + S_h \tag{8}$$

where E is the total energy, k_{eff} is the effective conductivity, and $\mathbf{j}_j$ is the diffusion flux of species j and h is the enthalpy, τ_{eff} is the effective stress tensor matrix and S_h is the source term per unit volume per unit time. However, the dissipation energy will be very low in the fuel cell due to low velocity laminar flow and can be omitted from the energy equation. The first three terms on the right-hand side of Eq. (8) represent the energy transfer due to conduction, species diffusion, and viscous dissipation, respectively.

2.3. Model equations in gas diffusion layers

The gas diffusion electrodes consist of carbon cloth or carbon fibre paper and can be considered as porous media through which reactant gases are distributed to the catalyst layer, while the solid matrix of the layer collects current and connects the reaction zone to the collector plates. Fig. 1 shows a schematic drawing of the cathode side of the fuel cell model, illustrating the transport of reactants, electrons and products.

The equations that govern gas transport phenomena in the diffusion layers are similar to those used in the channels with the addition of a porosity parameter. The mass conservation equation is expressed as:

$$\nabla \cdot (\rho \gamma \mathbf{v}) = S_{\text{m}} \tag{9}$$

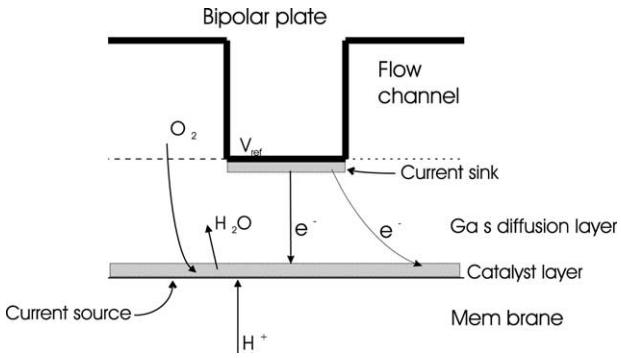

Fig. 1. Schematic of the cathode side.

in which γ is the porosity and S_{m} is a mass source, specified for the anode and cathode according to Eqs. (16) and (17) presented in Section 2.4.

In Fluent 6.1, a superficial velocity, based on the volumetric flow rate, is used inside the porous medium. This superficial velocity is also used to ensure continuity of the velocity vectors across the porous medium interface. More accurate simulations of porous media flows would require solution of the physical velocity throughout the flow-field, rather than the superficial velocity. Fluent 6.1 provides the possibility of solving the transport equation in the porous media using the physical velocity. However, the inlet mass flow is calculated from the superficial velocity and therefore the pressure drop across the porous media would be the same whether the physical or superficial velocity formulation is used.

The porous media model essentially consists of an extra momentum sink term added to the standard fluid flow Eq. (4). This source term consist of two loss terms, viscous and inertial:

$$S_{\text{mom},i} = -\left(\sum_{j=1}^{3} D_{ij} \mu v_j + \sum_{j=1}^{3} C_{ij} \frac{1}{2} \rho v_j v_j \right) \tag{10}$$

where $S_{\text{mom},i}$ is the source term for the momentum equation in the x, y or z direction, μ is the dynamic viscosity, C is the inertial resistance factor matrix and D is a matrix containing the inverse of the permeability, α. Note that the inertial loss term is only significant for high flow velocities, and its contribution is negligible in the present model. The momentum sink generates a pressure gradient in the porous region. The steady state momentum equation in the porous media using the physical velocity formulation can then be written as:

$$\nabla \cdot (\gamma \rho \mathbf{v}\mathbf{v}) = -\gamma \nabla \mathbf{p} + \nabla \gamma \tau - \frac{\mu}{\alpha} \mathbf{v} + S_{\text{mom}} \tag{11}$$

where γ and α are porosity and permeability respectively, and the other variables are defined as per Eq. (4).

2.3.1. Mass transport equation in porous media

The steady state species transport equation in porous media takes the form:

$$\nabla \cdot (\rho \gamma \mathbf{v} y_i) = \nabla \cdot (\rho \gamma D_i^{\text{eff}} \nabla y_i) + S_i \tag{12}$$

where the source term is given by Eqs. (16) and (17) for the anode and cathode gas diffusion layers, respectively. D_i^{eff} is an effective diffusion coefficient that takes into account the effect of additional drag by the irregular shape and the actual length of the pores in comparison with a bundle of straight parallel capillaries with constant diameter, and is given by [14,17]:

$$D_i^{\text{eff}} = \gamma \frac{D_i}{\mu_p} \tag{13}$$

where D_i is the diffusion coefficient, γ is the gas-phase porosity and μ_p is the tortuosity factor. The tortuosity factor can be split into a factor that accounts for the actual length of the channel μ_L, and a shape factor μ_F, ($\mu_p = \mu_L \mu_F^2$) [17]. It should be noted that the alternative Bruggemann correction which is frequently used is essentially equivalent for low tortuosities and porosities in the range 0.4–0.5. In this work, a tortuosity factor of 3 is used [14].

2.3.2. Energy transport in porous media

Eq. (8) is used to calculate the energy transport in the porous media with an effective thermal conductivity, k_{eff}, calculated as the volume average of the fluid conductivity and the solid conductivity (assuming thermodynamic equilibrium), i.e.:

$$k_{\text{eff}} = \gamma k_{\text{f}} + (1-\gamma) k_{\text{s}} \tag{14}$$

where k_{f} is the thermal conductivity in the fluid phase and k_{s} is the solid medium thermal conductivity.

2.3.3. Potential

The potential distribution in the gas diffusion layer can be calculated by applying the generic transport equation without the convective terms.

$$-\nabla \cdot (\sigma \nabla \phi) = S_\phi \tag{15}$$

where σ is the electronic conductivity. The source term, S_ϕ, is equal to the local current production which is given in Eq. (19), and ϕ is the local potential.

2.4. Catalyst layer

2.4.1. Mass sources and sinks

The local volumetric source and sink terms associated with the electrochemical reactions are proportional to the local current density:

$$S_{\text{H}_2}\,(\text{kg s}^{-1}\,\text{m}^{-3}) = -\frac{M_{\text{H}_2}}{2F} i \tag{16}$$

$$S_{\text{O}_2}\,(\text{kg s}^{-1}\,\text{m}^{-3}) = -\frac{M_{\text{O}_2}}{4F} i \tag{17}$$

$$S_{\text{H}_2\text{O}}\,(\text{kg s}^{-1}\,\text{m}^{-3}) = \frac{M_{\text{H}_2\text{O}}}{2F} i \tag{18}$$

where M_j are the molar masses to be, and F is Faraday's constant. Product water is assumed in vapour form. These source terms need to be included in both mass conservation and the transport equations.

2.4.2. Current calculations

The current density at both cathode and anode is calculated using the Butler–Volmer equation [18]:

$$i = i^+ + i^- = i_0 \left[\exp\left(\frac{\beta n F \eta}{RT}\right) - \exp\left(-\frac{(1-\beta) n F \eta}{RT}\right) \right] \tag{19}$$

where i_0 is the exchange current density, n is the number of electrons per mole of reactant, η is the local overpotential and R is the universal gas constant. β is the asymmetry parameter, which is determined empirically to be between 0.4 and 0.6 [18]. The sensitivity of the model to this parameter will be discussed subsequently.

The exchange current density is calculated from the following relations [13]:

Cathode:

$$i_0^+ = i_0^{\text{ref}_+} \left(\frac{c_{\text{O}_2}}{c_{\text{O}_2}^{\text{ref}}}\right)^{\gamma_{\text{O}_2}} \left(\frac{c_{\text{H}^+}}{c_{\text{H}^+}^{\text{ref}}}\right)^{\gamma_{\text{H}^+}^+} \tag{20}$$

Anode:

$$i_0^- = i_0^{\text{ref}_-} \left(\frac{c_{\text{H}_2}}{c_{\text{H}_2}^{\text{ref}}}\right)^{\gamma_{\text{H}_2}} \left(\frac{c_{\text{H}^+}}{c_{\text{H}^+}^{\text{ref}}}\right)^{\gamma_{\text{H}^+}^-} \tag{21}$$

where c_i is the concentration of species i, the superscript "ref" indicates a reference state, and γ is an empirically determined concentration parameter. For the cathode $\gamma_{\text{O}_2} = 1/2$ and $\gamma_{\text{H}^+} = 1/2$ [13]; and for the anode $\gamma_{\text{H}_2} = 1/4$ and $\gamma_{\text{H}^+} = 2$ [13].

In this model the concentration of protons at the catalyst surface of the cathode and anode is assumed constant. Eqs. (20) and (21) can then be simplified:

$$i_0^+ = k_{\text{c}} (c_{\text{O}_2})^{\gamma_{\text{O}_2}} (c_{\text{H}^+})^{\gamma_{\text{H}^+}^+} \tag{22}$$

$$i_0^- = k_{\text{a}} (c_{\text{H}_2})^{\gamma_{\text{H}_2}} \tag{23}$$

where k_{c} and k_{a} are experimentally determined constants that are dependent on the geometry of the catalyst layer.

No additional terms are required for mass transport losses, since these are accounted for in the exchange current density through the concentration term. When the overpotential due to mass transport losses is high, the concentration of reactants in the catalyst layer is low, and this results in a low local current density.

The dependence of the exchange current density on temperature is accounted for using the relation of Parthasarathy et al. (quoted by Fuller and Newman [19]):

$$i_0 = i_0(T_{\text{ref}}) \exp\left[\frac{\Delta E}{R}\left(\frac{1}{T_{\text{ref}}} - \frac{1}{T}\right)\right] \tag{24}$$

where ΔE is the activation energy ($\Delta E = 73.2\,\text{kJ mol}^{-1}$), and T_{ref} a reference temperature.

The activation overpotential stems from losses that are associated with the kinetics of the reactions taking place on the surface of the electrode. Activation losses are the most important irreversibility in low and medium temperature fuel cells [20]. When the reaction is not sufficiently fast to maintain the system in equilibrium at the surface, an activation overpotential needs to be taken into account. In many previous studies, a constant surface overpotential is assumed in order to linearize the Butler–Volmer equation. In this work, the local activation overpotential at the cathode is obtained from:

$$\eta_{\text{act}} = E_r - ir - V_{\text{input,cat}} \tag{25}$$

where ir represents the ohmic losses. $V_{\text{input,cat}}$ is the half-cell potential at the cathode side, which is an input parameter used in the model to specify the operating point of the cell. The reversible cell potential in Eq. (25), E_r, is obtained from the Nernst equation:

$$E_r = E^{\circ} - \frac{RT}{nF} \ln \left(\frac{a_{\text{H}_2\text{O}}}{a_{\text{O}_2}^{0.5} \times a_{\text{H}^+}^2 \times a_{\text{e}^-}^2} \right) \tag{26}$$

where E° is the open circuit voltage at standard pressure and a is the activity. It is assumed that the electrons are in their standard state and hence the activity is taken as 1.

The ohmic losses in Eq. (25) are obtained from solving the potential equation in the gas diffusion layer.

The activity of the protons in the membrane is difficult to specify. The concentration of protons is assumed to be constant in the membrane. This implies that the activity of the two half-cell reactions should be equal, and that the value of the proton activity will only influence the local heat production in the half-cell reactions. Bernardi and Verbrugge [13] refer to experimental measurements where the fixed-charge-site concentration in the membrane is found to be 1.2 mol dm^{-3}, which is almost equal to a 1 molar solution. In Ref. [21] the activity of protons in a 1 molar sulfuric acid, H_2SO_4, solution at 25 °C is given as 0.1316. Compared to other 1 molar solutions this is a low value and it is considered to be a worst case scenario. In this model the activity of protons is assumed constant and independent of temperature.

The activity of water vapour is given by:

$$a_{\text{H}_2\text{O}} = \frac{p_{\text{H}_2\text{O}}}{p_{\text{w,sat}}} \tag{27}$$

where $p_{\text{H}_2\text{O}}$ is the partial pressure of water vapour and $p_{\text{w,sat}}$ is the saturated water pressure.

The anodic activation overpotential is much smaller than the overpotential at the cathode [20]. Its local variation is therefore neglected, and a constant anodic overpotential is assumed in the present model. Due to current conservation, the average current density at the anode and cathode have to be equal. Hence the anodic overpotential can be found by applying an algorithm which calculates the Butler–Volmer equation using a value for the overpotential that provides an average current density at the anode equal to that at the cathode.

The total cell potential for the fuel cell is calculated in the post-processing:

$$E^{\text{cell}} = E_{\text{cathode}} - E_{\text{anode}} - \eta_{\text{mem}} - \eta_{\text{contact}} \tag{28}$$

where E_{cathode} is set equal to $V_{\text{input,cat}}$, the input cathode half-cell potential, E_{anode} is the anodic half-cell potential (reversible cell potential minus overpotentials at the anode), η_{mem} is the potential loss in the membrane, and η_{contact} is the contact resistance.

2.4.3. Heat sources and sinks

The heat generated in a fuel cell is due to changes of enthalpy and irreversibilities related to charge transfer. In order to calculate the heat generation, both charged and non-charged species need to be considered. Values for the entropy of electrons and protons are required for the computation. Lampinen and Fomino [22,23] presented a method of calculating ΔG, ΔH and ΔS for each half-cell reaction. Implementing this approach allows resolution of the heat generation between the cathode and anode, and a more accurate prediction of the temperature profile in the fuel cell.

The energy balance for a half-cell can be written as [22]:

$$\dot{Q} = r\Delta H + P_{\text{el}} \tag{29}$$

where $\dot{Q}$ is the heat absorbed, r is the reaction rate of the half-cell reaction, ΔH is the half-cell reaction enthalpy and P_{el} is the electric power. The half-cell heat production/absorption for a real process can be shown to be [22,24]:

$$\dot{q} = |i/nF|(\Delta H + (-\Delta G)) - |i||\eta| = |i/nF|(T\Delta S) - |i||\eta| \tag{30}$$

where n is the number of electrons per mole of reactants, ΔH, ΔG and ΔS are the half-cell changes in enthalpy, Gibbs free energy and entropy, respectively, i is the local current density, η is the voltage drop (overpotential) due to ohmic losses and reaction resistance, and F is Faraday's constant. The entropy change at standard state with platinum catalyst is taken as $\Delta S = 0.104\,\text{J mol}^{-1}\,\text{K}^{-1}$ for the anode side, and $\Delta S = -326.36\,\text{J mol}^{-1}\,\text{K}^{-1}$ for the cathode side [22,24].

2.5. Membrane

The polymer electrolyte membrane acts primarily as a material barrier between the anode and cathode reactants, and as a protonic conductor. Both water and heat are also transported through the membrane.

2.5.1. Potential field and heat transfer

Electro-neutrality is assumed to prevail inside the membrane. Following Bernardi and Verbrugge [25], proton concentration within the membrane is assumed to be constant and equal to the concentration of fixed sulfonic acid groups. This is a valid assumption for a fully humidified membrane, however, in future work, approaches similar to those used for

calculating charges in semiconductors should be considered for computing the concentration of protons in the membrane.

Heat conduction through the membrane is represented by Eq. (8), without any convective or source terms.

The potential field in the membrane is computed using

$$-\nabla \cdot (\kappa \nabla \phi_{\mathrm{m}}) = 0 \tag{31}$$

where κ is the ionic conductivity, and ϕ_{m} is the ionic potential in the membrane. Eq. (31) is solved subject to a constant potential at the anode and a distributed flux at the cathode (see Section 3.3 for description of boundary conditions).

The ionic conductivity is dependant on water content, λ, in the membrane. For a fully humidified membrane values between 14 and 16.8 are reported [26]. In this model a constant value of 15 is used, and the conductivity is obtained using the empirical model of Springer et al. [26], yielding a conductivity of 13.375 S m^{-1}.

2.5.2. Water transport in the membrane

The current model considers only operation under fully humidified conditions. It is common to distinguish between three water transport mechanisms in polymer membranes: electro-osmosis, diffusion and convection. The model used here is based on the approach of Janssen [28], where rather than prescribing specific transport mechanisms individually, fundamental thermodynamic considerations are used to account for all the different mechanisms through a chemical potential [28]:

$$j = -L_{++}\nabla \phi_{\mathrm{m}} - L_{+\mathrm{w}}\nabla \mu_{\mathrm{w}} \tag{32}$$

$$N_{\mathrm{w}} = -L_{\mathrm{w}+}\nabla \phi_{\mathrm{m}} - L_{\mathrm{ww}}\nabla \mu_{\mathrm{w}} \tag{33}$$

where j is the current density of protons, ϕ_{m} is the local potential, μ_{w} is the local chemical potential of water and the L variables are Onsager coefficients.

The physical interpretation of L_{++} is the specific proton conductivity, κ [28]. According to Onsager relations $L_{+\mathrm{w}} = L_{\mathrm{w}+}$. It can be shown that $L_{\mathrm{w}+} = \frac{\xi\kappa}{F}$ [28], in which ξ is the number of water molecules transported with each proton. Further discussion and physical interpretation of L_{ww} is provided in Sivertsen [24].

In Janssen's model, Eqs. (32) and (33) are combined in order to express the water flux in terms of the current density of protons:

$$N_{\mathrm{w}} = t_{\mathrm{w}} j - l_{\mathrm{mem}}\nabla \mu_{\mathrm{w}} \tag{34}$$

in which

$$t_{\mathrm{w}} = \frac{L_{\mathrm{w}+}}{L_{++}} \tag{35}$$

$$l_{\mathrm{mem}} = L_{\mathrm{ww}} - \frac{L_{+\mathrm{w}}L_{+\mathrm{w}}}{L_{++}} \tag{36}$$

The parameter t_{w} is a measure of the electro-osmotic drag and the term $l_{\mathrm{mem}}\nabla\mu_{\mathrm{w}}$ is related to the back transport of water in the membrane. Values for l_{mem} for different membranes are given by Janssen [28]. In this model l_{mem} is assumed to be constant. This is consistent with the fully humidified membrane assumption [28].

3. Boundary conditions

Boundary conditions are required at all boundaries of the computational domains, as well as at internal interfaces.

3.1. Inlet conditions

At the inlet of both anode and cathode flow channels the boundary values are prescribed from the stoichiometric flow rate, temperature and mass fractions. The mass flow rate at the inlet is prescribed in conjunction with a fully developed laminar flow profile. Exact solutions for such profiles are available for a variety of cross-sectional areas, but we found it computationally more effective to use an approximation which provides values within 1% of the exact solution [29]:

$$u = u_{\max}\left(1 - \left(\frac{y}{b}\right)^n\right)\left(1 - \left(\frac{z}{a}\right)^m\right) \tag{37}$$

$$u_{\max} = u_m\left(\frac{m+1}{m}\right)\left(\frac{n+1}{n}\right) \tag{38}$$

where $u_{\max}$ is the maximum velocity, a is the half-width of a non-circular duct, b is the half-height of a non-circular duct and u_m is the average velocity. Relations for the values m and n are [29]:

$$m = 1.7 + 0.5\left(\frac{a}{b}\right)^{-1.4}$$

$$n = \begin{cases} 2, & \text{for } \frac{a}{b} \le \frac{1}{3} \\ 2 + 0.3\left(\frac{a}{b} - \frac{1}{3}\right), & \text{for } \frac{a}{b} \ge \frac{1}{3} \end{cases}$$

The model was implemented to allow the option of having fully humidified inlet reactant flows. The saturation pressure for water vapour is given as a quartic equation developed using a regression of tabulated values from Moran and Shapiro [30].

$$\begin{aligned} p_{\mathrm{w,sat}}\,(\mathrm{Pa}) = (&1.268366 \times 10^{-8} \times T^4 - 1.498267 \times 10^{-5} \\ &\times T^3 + 0.0067091643 \times T^2 - 1.348318703 \\ &\times T + 102.5034101) \times 10^5 \end{aligned} \tag{39}$$

This equation is valid for temperatures from 323.15 to 383.15 K (50–110 °C).

3.2. Outlet conditions

The momentum equation solver in Fluent uses a pressure correction method which does not allow specification of two different reference pressures in the computational domain.

Since the reactant gas flow channels are separate and generally at different pressures, pressure boundary conditions are used at the outlets.

3.3. Boundary conditions at internal interfaces

3.3.1. Interface between the electrode and the flow channel

At the interface between the electrode and the flow channel, a user defined function (UDF) was implemented to enforce a zero flux of electrons. This is done by overwriting the value of the potential in the first cell in the flow-channel side of the interface with the same value as the adjacent cell on the electrode side, thereby enforcing a zero potential gradient normal to the interface.

3.3.2. Interface between the electrode and the membrane

Due to the structure of the Fluent CFD code, the interface between the membrane and the electrodes is defined as a wall (impermeable boundary). This is done mainly to prevent any crossover of species and electrons through the membrane, but also to prevent pressure related problems. The wall has a fluid region on each side, and each side is therefore treated as a distinct wall. This is implemented by creating a "shadow" of the wall cell layer. The "walls" are thermally coupled, such that heat transfer can be directly computed from the solution in the adjacent cells, and hence no additional boundary conditions is required for the energy equation. The use of an internal wall is an expedient way of implementing our model in Fluent and it is physically consistent, but more straightforward alternatives should be explored.

The potential profile in the membrane is solved by setting the ionic potential to zero at the anode side interface between the catalyst and the membrane. This is based on the assumption that the potential at the anode side is uniform. At the membrane–catalyst interface on the cathode side, a negative flux equal to the consumption of protons in the adjacent cell in the catalyst layer is specified.

As described earlier, the gradient of the chemical potential is used to calculate the water flux through the membrane. The profile of the chemical potential in the membrane is computed using the water transport equation subject to specified values at the membrane/electrode interfaces. Local equilibrium is assumed at the interfaces, i.e. the water in the membrane and the water vapour in the electrode are in equilibrium. The boundary conditions at the anode and cathode interfaces are [28]:

$$\mu_{\mathrm{w}}^{\mathrm{mem}} = \mu_{\mathrm{w}}^{0} + RT \ln \frac{p_{\mathrm{w}}}{p^{0}} \tag{40}$$

where $\mu_{\mathrm{w}}^{\mathrm{mem}}$ is the chemical potential of water vapour in the membrane at the interface, μ_{w}^{0} is the chemical potential at standard conditions, p_{w} is the water vapour pressure in the electrode at the interface, and p^{0} is the standard pressure.

3.4. Land areas

In the areas where the gas diffusion electrodes are in contact with the bipolar plates (the land area) a constant reference voltage equal to zero is applied as a boundary condition both at the anode and at the cathode. At all other walls, the electron flux is set to zero.

3.5. Walls

On all walls the no-slip boundary condition is applied for the momentum equations.

Different boundary conditions for the energy equation can be employed: specified heat flux, temperature or convective heat transfer. The specific boundary condition will be presented with each of the cases investigated in this paper.

4. Computational procedure

The governing transport equations are solved subject to the various boundary conditions presented in the preceding section using the Fluent 6.1 [12] CFD code. Fluent 6.1 is a parallel code using a finite volume method and an iterative segregated implicit solver. Second order discretization schemes are utilized for all transport equations (i.e. central differencing for diffusion terms, and second order upwind for convection terms).

The model equations specific to physico-chemical transport in PEM fuel cells presented earlier were implemented using a set of UDFs written in C and dynamically linked with the Fluent source code. These UDFs were developed such as to maintain the parallel computing capabilities which significantly enhances the useability of the code for problems necessitating a large number of computational nodes. Another important feature of the model presented here is an iterative voltage–current algorithm also implemented using UDFs. This algorithm allows prediction of the cell current density based on a target cell operating voltage, and does not require the assumption of a specific constant overpotential over the entire cell, but rather allows prediction of the spatial variation of the *local* surface overpotential.

5. Test case geometry and parameters

The geometry, parameters and operating conditions used in the simulations correspond to the experimental test case of Wang et al. [31]. It is common to compare results from model predictions with polarization curves obtained from experiments or other models. This is not a very satisfactory way of verifying model performance. Until progress is made in the difficult problem of obtaining detailed and reliable in situ experimental data, we will continue to use polarization curves and complement the assessment with an analysis of the physical results obtained with the model. Given the state

of development of PEM fuel cell modelling, the complexity of the transport phenomena, and the large range of physical scales involved, and the uncertainty in determining some of the physico-chemical parameters, it is any case unrealistic to expect accurate quantitative agreement between experiments and computational model simulations. Simulation based on physically representative models should however yield correct relative trends and provide valuable insight and guidance for design and optimization.

The geometry of the fuel cell simulated in this work is a straight section consisting of bipolar plates with flow channels separated by a membrane–electrode assembly. The dimensions of the fuel cell section are given in Table 1 and correspond to the experimental test case of Ref. [31]. A non-uniform grid was used to minimize the computational requirements while allowing proper resolution in high gradient regions (near wall regions; porous electrodes). It should be noted that though the implementation allows for the resolution of the catalyst layer, the simulations presented here use a single computational layer for the catalyst layer.

A grid sensitivity study was performed to establish the grid resolution requirements. Three meshes with 546,000 (grid A), 155,925 (grid B) and 66,240 (grid C) computational cells each were generated. At a cell potential of 0.798 V, the coarsest grid C and the medium grid B yield deviations of about 1.2% and 0.9% for the average current density compared to the fine grid A. All simulations presented here were performed using the finest grid in which the anode and the cathode flow channel are each divided into $20 \times 18 \times 150$ grid cells; the membrane into $40 \times 7 \times 150$ computational cells; and the gas diffusion layers into $40 \times 12 \times 150$ cells. The catalyst layers thickness consists of one computational volume, i.e. a total of $40 \times 1 \times 150$ cell each. It should be noted that the parallel solver allows us to use a large computational grid (total of 546,000 cells) that allows much finer resolution than those employed in previous work (e.g. [5,6]).

Table 2 provides the basic experimental operating conditions [31] used for the simulations. Since the computational domain does not include a serpentine flow channel, the mass flow rate is adjusted to maintain a stoichiometry of 3. The reactants are assumed to be fully humidified at the inlets (Table 3).

The gas diffusion layer and membrane properties used in the base case simulations are given in (Tables 4 and 5). In the literature, the asymmetry parameter β (also referred to as the transfer coefficient) is ascribed values ranging from

Table 1
Physical dimensions for the straight channel fuel cell section

Parameter	Value	Unit
Cell width	2.0×10^{-3}	m
Channel length	0.07	m
Channel height	1.0×10^{-3}	m
Channel width	1.0×10^{-3}	m
Land area width	1.0×10^{-3}	m
Electrode thickness	0.3×10^{-3}	m
Catalyst layer thickness	1.29×10^{-5}	m
Membrane thickness	0.108×10^{-3}	m

Table 2
Operation parameters for the straight channel fuel cell section

Parameter	Value	Unit
Inlet temperature, anode and cathode	80	°C
Anode side pressure	3	atm
Cathode side pressure	3	atm
Anode stoichiometric flow rate	3	–
Cathode stoichiometric flow rate	3	–
Relative humidity of inlet gases	100	%
Oxygen/nitrogen ratio	0.79/0.21	–

Table 3
Inlet mass fraction (fully humidified flow)

Species	Mass fraction (%)
H_2O, anode	62.253
H_2, anode	37.747
H_2O, cathode	10.344
O_2, cathode	20.885
N_2, cathode	68.771

Table 4
Electrode properties

Parameter	Symbols	Value	Unit	Reference
Electrode porosity	γ	0.4	–	[31]
Permeability	α	1.76×10^{-11}	m^2	[31]
Tortuosity	μ_p	3.0	–	[14]
Thermal conductivity				
Solid region	k	150.6	$W\,m^{-1}\,K^{-1}$	[6]
Electronic conductivity	σ	100	$S\,m^{-1}$	[36]
Asymmetry parameter				
Anode	β	0.5	–	[18]
Cathode	β	1.0/0.5	–	[13,18,32]
Concentration parameter				
Hydrogen	γ_{H_2}	0.25	–	[13]
Oxygen	γ_{O_2}	0.5	–	[13]
Constant, anode	k_a	17.00×10^7	–	–
Constant, cathode $\beta = 1.0$	k_c	40.75×10^{-11}	–	–
Constant, cathode $\beta = 0.5$	k_c	0.8093958	–	–

Table 5
Membrane properties

Parameter	Symbols	Value	Unit	References
Thermal conductivity	k	0.67	$\mathrm{W\,m^{-1}\,K^{-1}}$	[6]
Proton conductivity	κ	13.375	$\mathrm{S\,m^{-1}}$	[26]
Permeability in the membrane	l_{mem}	2.35×10^{-7}	$\mathrm{mol^2\,s\,m^{-3}\,kg^{-1}}$	[28]
Fixed-charge concentration	$c_{\mathrm{H^+}}$	1200	$\mathrm{mol\,m^{-3}}$	[13]
Number of water molecules Transported per proton	ξ	3	–	[28,27]

1 to 0 [32]. Because of this variability, a parametric study was undertaken to assess the effect of the asymmetry parameter at the cathode, where this parameter was varied for 0.5 to 1.0.

It should be noted that the value given by Bernardi and Verbrugge [13] for the transfer coefficients at the anode, is not strictly consistent with the Butler–Volmer equation [18,32] which requires that the coefficients for the forward and backward components of should add to unity. The values for transfer coefficients at the anode given by Bernardi and Verbrugge [13], which also was used by Wang et al. [31], is therefore not used in this model. However, since the activation overpotential at the anode is much smaller than that at the cathode, the value of the charge transfer coefficients at the anode is of less importance.

A constant temperature of 80 °C is applied as a boundary condition to the outer walls of the fuel cell. The thermal conductivity of the bipolar plates is set to $35\,\mathrm{W\,m^{-1}\,K^{-1}}$ and the electrical resistance is set to $50 \times 10^{-6}\,\Omega\,\mathrm{m}$, which are a mid-range values for the data presented by Middelman et al. [33]. In the experiments of Wang et al. [31] gold-plated copper plate were used to connect the bipolar-plates with the external circuit; the electrical contact resistance is consequently set to zero in the computational model.

All other properties used for the fluids and solids are taken from Mills [34].

6. Results and discussion

The results obtained for the straight channel case is presented and discussed in this section. All computations were preformed on a Linux computer cluster with dual 2000+ AMD Athlon processors on each node. The maximum number of processors used were eight. The number of iterations required and the computation time was dependent on the initial conditions specified and the input of the cathode half-cell voltage.

6.1. Polarisation curve and effect of asymmetry parameter

Good agreement between measured and computed polarisation curves is not sufficient to assess the predictive capabilities of a model, but is a prerequisite. In order to investigate the effect of the asymmetry parameter on the polarisation curve, simulations were performed for $\beta = 1.0$ and 0.5. Fig. 2 compares the computed and measured polarisation curves.

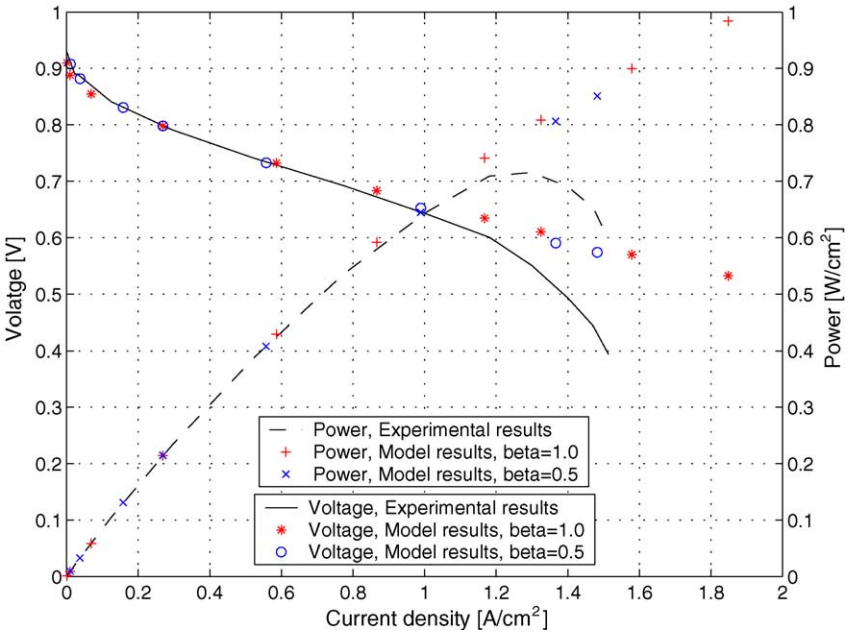

Fig. 2. Polarisation curve: comparison of simulations and experiments [31].

In the activation and the ohmic region (low and mid-range current densities) of the polarisation curve, the results from the model are in good agreement with experiments, with deviations of less than 5.0% for $\beta = 1.0$ and less than 1.1% with $\beta = 0.5$. At very low current densities the simulations with $\beta = 0.5$ appear to follow the experimental results better than the simulations with $\beta = 1.0$. This suggests the actual value of the asymmetry parameter should be closer to 0.5 than 1.0, which is consistent with the range of values reported by Hamann et al. [18].

As expected, the model is unable to reproduce the experimental data at high current densities. The discrepancy in this region is attributed in part to the assumption of single phase transport. In practice, however, the formation of liquid is expected to limit mass transport at higher current densities [8]. Another effect that may lead to a drop in the cell voltage at higher current densities, is the shift of the reaction zone in the catalyst layer away from the membrane interface at higher currents [9]. The protons need to be transported further out in the catalyst layer due to depletion of oxygen in the catalyst, and this lead to increased ohmic losses. This effect is not resolved here since the catalyst is modelled as a single layer of computational cells.

Fig. 3 shows the local current distributions obtained in the cathode catalyst layer for two values of asymmetry parameter, $\beta = 1.0$ and 0.5. The $\beta = 1.0$ case exhibits markedly higher peaks in the shoulders near the inlet. The relative difference between the two case is shown in Fig. 4. The difference in the current density profiles can be explained by the fact that for any given activation overpotential, the Butler–Volmer equation yields a higher current density for a higher value of the asymmetry parameter, and hence the current density profile will exhibit larger maxima. Since the average current density is the same in both cases, the total oxygen consumption is also the same. Whereas the difference in the local current density is greater than 18% at some locations, the cathode half-cell potential and the cell potential are virtually identical (maximum deviation less than 0.2%). This result shows that even though the results obtained for the two asymmetry parameters yield identical data on the polarization curve, the current distributions are significantly different. The prediction of physically representative distributions is important in practice as non-uniformity can have a significant impact on the design and longevity of a fuel cell.

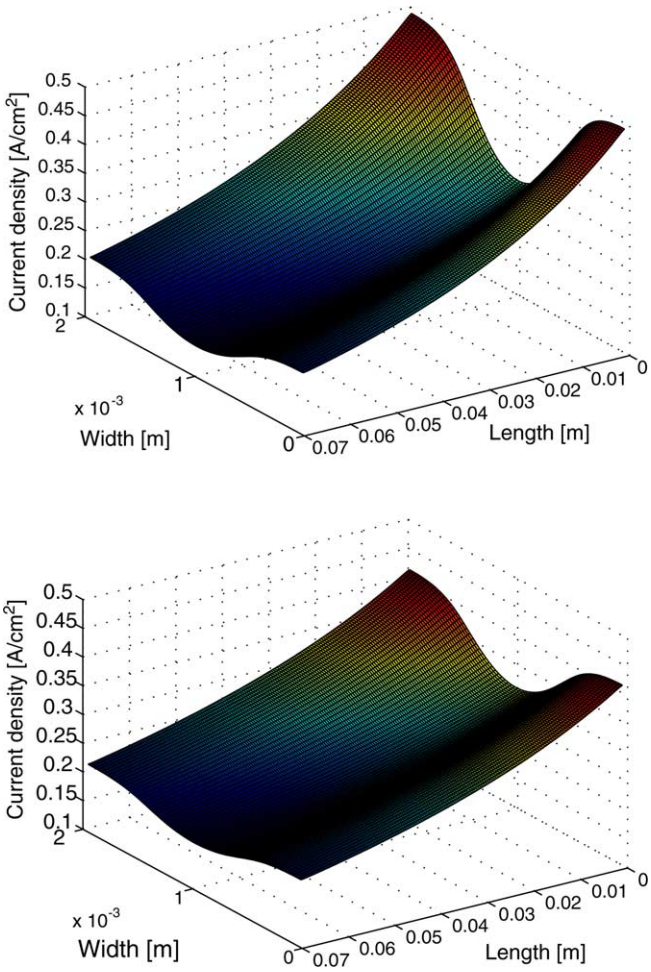

Fig. 3. Effect of asymmetry parameter on cathodic current density distribution at i_{avg} 0.269 A cm^{-2}. Top: $\beta = 1.0$; bottom: $\beta = 0.5$.

6.2. Relative influence of activation and ohmic losses

Figs. 5 and 6 present the current density, activation overpotential and oxygen mass fraction distributions for two current densities, $i_{avg} = 0.269$ and 0.989 A cm^{-2}. For the lower load case, cathode activation overpotential and the local current density are fairly uniform, but both vary much more in the higher load case. Both figures show that the current density profiles correlate with the activation overpotential, but not with the oxygen concentration. These results are radically different from the intuitively expected profiles and from predictions obtained with models assuming constant overpotential (e.g. [6]), where the current densities are highest in the centre of the channel and coincide with the highest reactant concentrations. The present results are also consistent with

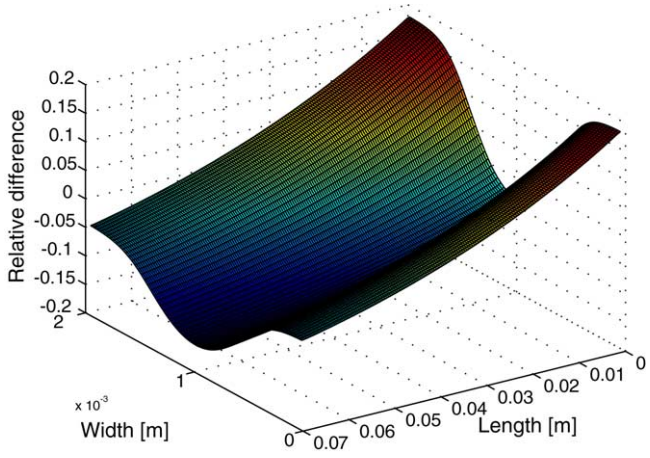

Fig. 4. Relative difference between the computed current density profiles with $\beta = 1.0$ and $\beta = 0.5$ (reference $\beta = 0.5$).

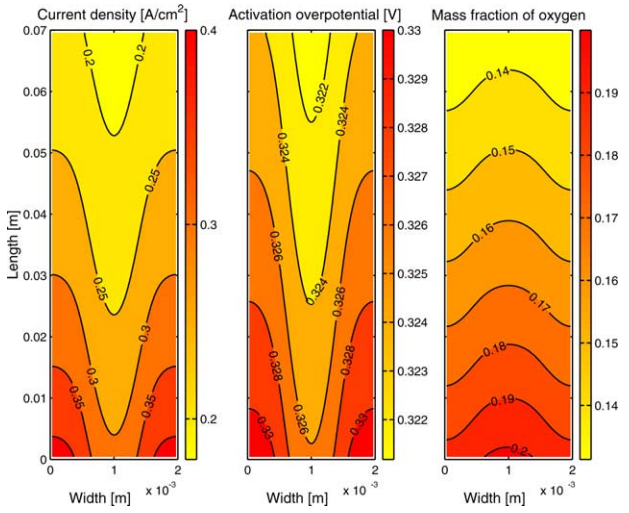

Fig. 5. Isocontours for current density, activation overpotential and oxygen mass fraction at the cathode catalyst layer at $V = 0.798$ V, $i_{avg} = 0.269$ A cm^{-2}, $\beta = 0.5$.

recent studies where distributed activation potential and complete charge transport are accounted for [9,35].

The current density maxima under the land areas is associated with the fact that ohmic losses in the gas diffusion layer influence the activity at the catalyst more than the concentration losses. The electric current path from the area of the catalyst layer under the flow channel is longer than the path from the area of the catalyst layer under the land areas (see Fig. 1). The potential field in the cathodic and the anodic gas diffusion electrodes are shown in Fig. 7 at the middle plane of the cell. The isopotential lines are normal to the flow channel and the side walls, while there is a gradient into the land areas where electrons flow into the bipolar plate. The distributions exhibit gradients in both x and z direction due

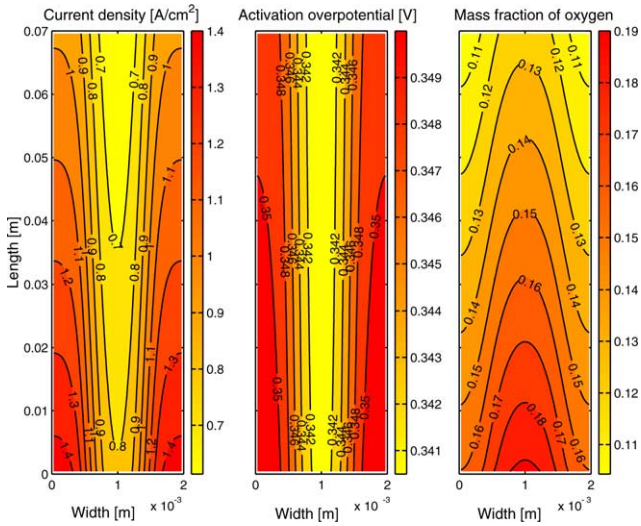

Fig. 6. Isocontours for current density, activation overpotential and oxygen mass fraction at the cathode catalyst layer at $V_{ref} = 0.652$ V, $i_{avg} = 0.989$ A cm^{-2}, $\beta = 0.5$.

to the non-uniform local current production and show that ohmic losses are larger in the area of the catalyst layer under the flow channels. Note that the potential along the anode side interface (bottom) is assumed uniform and is the reference potential ($V_{mem} = 0$ V).

Since the conductivity of the gas diffusion layer is expected to have a strong influence on the activation overpotential, and hence on the current distribution, parametric simulations for several conductivities were performed to assess this effect. Fig. 8a–c shows the changes in the profiles when the resistance in the gas diffusion layer is reduced. Since the fuel cell will operate at different loads (fixed cathode half-cell potential) when the conductivity in the gas diffusion electrode is changed, relative current density profiles are examined. Results are presented for three conductivity values while maintaining all other parameter constant: 100 S m^{-1} [36], 825 S m^{-1} [9] and 1500 S m^{-1}. With increasing electronic conductivity (or reduced electrode thickness), ohmic losses through the electrode decrease, the concentration losses become larger relative to the ohmic losses, and the local current density maxima shift toward the centre of the channel where the losses are smallest.

6.3. Further discussion

The potential distribution in the fuel cell has been shown to govern the current density distribution. In this study, effects associated with two-phase flow have not been considered. These might have a large impact on the actual current profile at higher current densities, and liquid water pockets are more likely to form under the land area of the gas diffusion layer [37,8]. This would inhibit the diffusion of the reactant to the catalyst layer and thereby reduce the current density in this area, thus counterbalancing some of the trends reported in this study. For simulations corresponding to intermediate current densities, where condensation is not expected to play a significant role, the result reported here are expected to be physically representative.

In this work the gas diffusion layer was assumed to be homogeneous and isotropic, whereas actual carbon paper materials commonly used to fabricate gas diffusion electrodes are anisotropic, and the permeability is likely to be lower in the plane of the carbon paper layer than across it. The species transport in the in plane directions would thus be expected to be lower than in the direction perpendicular to the gas diffusion layer. A potentially more important effect of the non-isotropic gas diffusion layer is that the tortuosity factor could be different in the two directions, leading to a lower diffusion into the areas under the land areas. Accounting for the anisotropic properties of the gas diffusion layer would likely yield lower concentration of reactant gas under the land area, and hence, lower local current densities in this area. There are no fundamental difficulties in accounting for the anisotropic properties in the CFD model, the problem is rather in obtaining reliable data in prescribing the properties.

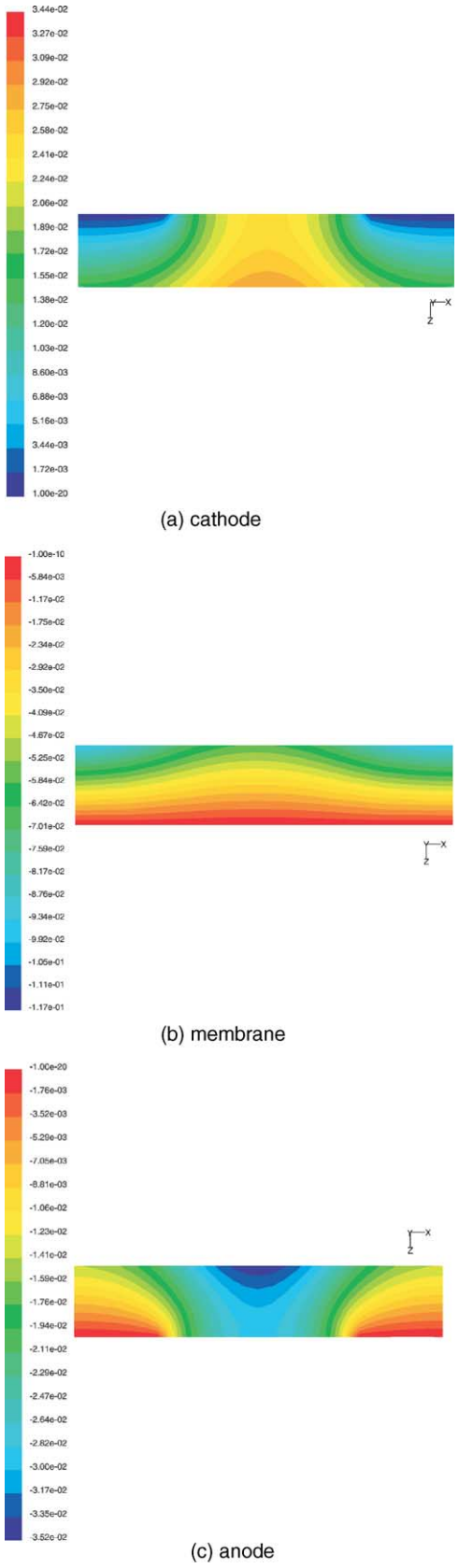

Fig. 7. Cross-section contours of the potentials in the MEA at a midway location in the channel ($V = 0.652$ V, $i_{avg} = 0.989$ A cm^{-2}, $\beta = 0.5$). (a) Cathode, (b) membrane, and (c) anode.

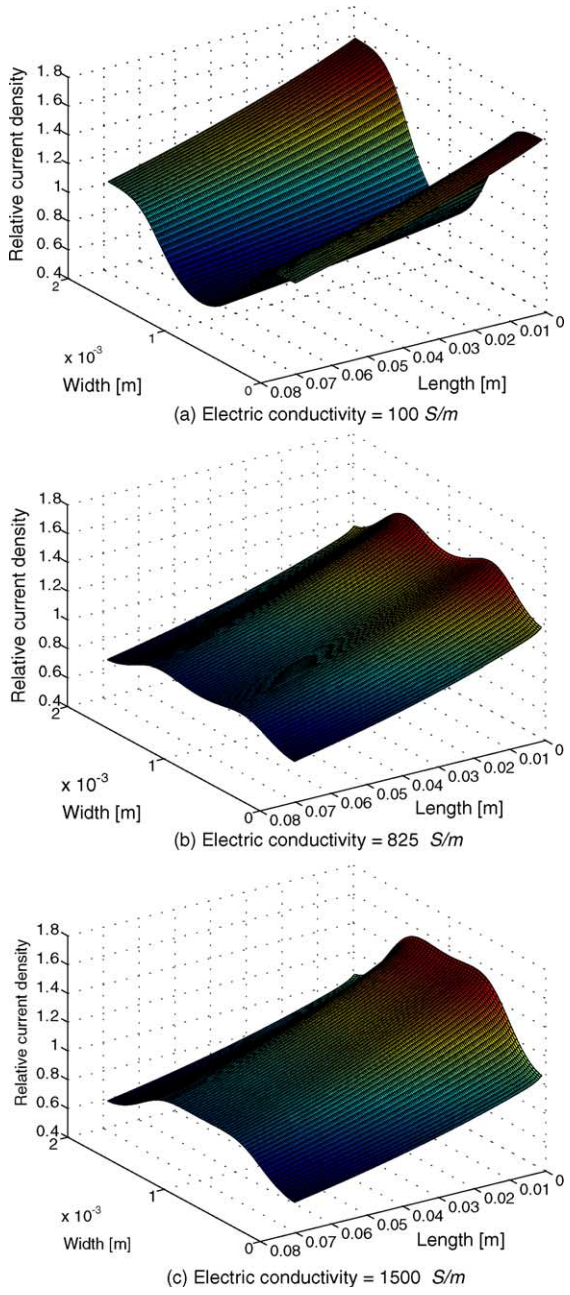

Fig. 8. Plots of the relative current densities (i_{local}/i_{avg}) for different conductivities ($i_{avg} = 0.269$ A cm^{-2}; $V = 0.798$ V; $\beta = 0.5$). Electric conductivity: (a) 100 S m^{-1}, (b) 825 S m^{-1}, and (c) 1500 S m^{-1}.

6.4. Conclusions

A three-dimensional model of a proton exchange membrane fuel cell has been developed and implemented in the framework of a CFD code. The model implementation takes advantage of the parallel processing architecture of the Fluent CFD code, thus allowing fast simulations even with fine grid resolution and/or large computational domains. The grid resolution used in this study is significantly finer than those reported in previous computational work. The model accounts

for the fluid transport inside the channels and the gas diffusion electrodes as well as heat transfer. The cathodic overpotential distribution is resolved, rather than assumed uniform and constant, allowing more accurate predictions of local current densities.

Global comparisons show good agreement between the model and experimental results. The computational analysis shows that substantially different spatial distributions can be obtained by varying the asymmetry parameter with no noticeable change in the polarization curves. This further highlights that global comparison between experimental and predicted results is, as pointed out in previous studies, insufficient to validate computational model. Detailed experimental data providing spatially resolved distributions of key quantities is essential for proper validation.

The predicted distribution of current densities show profiles which are fundamentally different from the distribution obtained in multi-dimensional models that do not account for distributed overpotentials. The maximum current density occurs under the land areas as a result of the dominant influence of ohmic losses over concentration losses on the activity at the catalyst layer. The study shows that changing the conductivity radically alters the current distribution by changing the relative influence of ohmic to activation overpotentials.

Acknowledgments

The support and input of Prof. Ole Melhus at the Norwegian University of Science and Technology, NTNU, is gratefully acknowledged. This work was funded by a Discovery grant to ND from Science and Engineering Research Canada (NSERC).

References

[1] V. Gurau, H. Liu, S. Kakaç, Two-dimensional model for proton exchange membrane fuel cells, AIChE J. 44 (11) (1998) 2410–2422.
[2] D. Singh, D.M. Lu, N. Djilali, A two-dimensional analysis of mass transport in proton exchange membrane fuel cells, Int. J. Eng. Sci. 37 (4) (1999) 431–452.
[3] S. Dutta, S. Shimpalee, J.W. Van Zee, Three-dimensional numerical simulation of straight channel PEM fuel cells, J. Appl. Electrochem. 30 (2000) 135–146.
[4] S. Um, C.Y. Wang, C.S. Chen, Computational fluid dynamics modeling of proton exchange membrane fuel cells, J. Electrochem. Soc. 147 (12) (2000) 4485–4493.
[5] S. Dutta, S. Shimpalee, J.W. Van Zee, Numerical prediction of mass-exchange between cathode and anode channels in a PEM fuel cell, Int. J. Heat Mass Transfer 44 (2001) 2029–2042.
[6] T. Berning, D.M. Lu, N. Djilali, Three-dimensional computational analysis of transport phenomena in a PEM fuel cell, J. Power Sources 106 (2002) 284–294.
[7] T. Zhou, H. Liu, A general three-dimensional model for proton exchange membrane fuel cells, Int. J. Transport Phenomena 3 (2001) 177–198.
[8] T. Berning, N. Djilali, A 3D, multi-phase, multicomponent model of the cathode and anode of a pem fuel cell, J. Electrochem. Soc. 150 (12) (2003) A1589–A1598.
[9] M. Bang, S. Yde-Andersen, T.J. Condra, N. Djilali, E. Skou, Modelling of potential fields and electrochemical reactions in PEM fuel cells, Proceedings of Hydrogen and Fuel Cells 2003 Conference, Vancouver, 2003, pp. 11–22.
[10] P.T. Nguyen, T. Berning, N. Djilali, Computational model of a pem fuel cell with serpentine gas flow channels, J. Power Sources 130 (1/2) (2004) 149–157.
[11] H. Meng, C.Y. Wang, Electron transport in pefcs, J. Electrochem. Soc. 151 (3) (2004) A358–A367.
[12] Fluent Incorporated, Fluent 6.0 and 6.1 User's Guide, 2001.
[13] D.M. Bernardi, M.W. Verbrugge, A mathematical model of the solid-polymer-electrolyte fuel cell, J. Electrochem. Soc. 139 (9) (1992) 2477–2491.
[14] E.L. Cussler, Diffusion Mass Transfer in Fluid Systems, second ed., Cambridge University Press, 1997.
[15] R. Taylor, R. Krishna, Multicomponent Mass Transfer, John Wiley & Sons, 1993.
[16] F.P. Incropera, D.P. DeWitt, Fundamentals of Heat and Mass Transfer, fourth ed., John Wiley & Sons, 1996.
[17] W. Kast, C.-R. Hohenthanner, Mass transfer within the gas-phase of porous media, Int. J. Heat Mass Transfer 43 (2000) 807–823.
[18] C.H. Hamann, A. Hamnett, W. Vielstich, Electrochemistry, Wiley-VCH, 1998.
[19] T.F. Fuller, J. Newman, Water and thermal management in solid-polymer-electrolyte fuel cells, J. Electrochem. Soc. 140 (5) (1993) 1218–1225.
[20] J. Larminie, A. Dicks, Fuel Cell Systems Explained, John Wiley & Sons, 2000.
[21] R.C. Weast (Ed.), CRC Handbook of Chemistry and Physics, 70th ed., CRC Press, Inc., 1989.
[22] M.J. Lampinen, M. Fomino, Analysis of free energy and entropy changes for half-cell reactions, J. Electrochem. Soc. 140 (12) (1993) 3537–3546.
[23] M.J. Lampinen, M. Fomino, Analysis of different energy scales in chemical thermodynamics and estimation of free energy and enthalpy changes for half cell reactions, Acta Polytech. Scand., 1993 (Chemical Technology and Metallurgy Series No. 213, Helsinki 1993).
[24] B.R. Sivertsen, CFD-based modelling of proton exchange membrane fuel cells. Master's thesis, Norwegian University of Science and Technology, 2003.
[25] D.M. Bernardi, M.W. Verbrugge, Mathematical model of gas diffusion electrode bonded to a polymer electrolyte, AIChE J. 37 (8) (1991) 1151–1163.
[26] T.E. Springer, T.A. Zawodzinski, S. Gottesfeld, Polymer electrolyte fuel cell model, J. Electrochem. Soc. 138 (8) (1991) 2334–2342.
[27] Y. Sone, P. Ekdunge, D. Simonsson, Proton conductivity of Nafion 117 as measured by a four-electrode AC impedance method, J. Electrochem. Soc. 143 (4) (1996) 1254–1259.
[28] G.J.M. Janssen, A phenomenological model of water transport in a proton exchange membrane fuel cell, J. Electrochem. Soc. 148 (12) (2001) A1313–A1323.
[29] S. Kakaç, R.K. Shah, W. Aung (Eds.), Handbook of Single-Phase Convective Heat Transfer, John Wiley & Sons, 1987.
[30] M.J. Moran, H.N. Shapiro, Fundamentals of Engineering Thermodynamics, John Wiley & Sons, 1996.
[31] L. Wang, A. Husar, T. Zhou, H. Liu, A parameteric study of PEM fuel cell performances, Int. J. Hydrogen Energy 28 (2003) 1263–1272.

[32] A.J. Bard, L.R. Faulkner, Electrochemical Methods, Fundamentals and Applications, second ed., John Wiley & Sons, 2001.
[33] E. Middelman, W. Kout, B. Vogelaar, J. Lenssen, E. de Waal, Bipolar plates for PEM fuel cells. J. Power Sources 118 (2003) 44–46.
[34] A.F. Mills, Heat Transfer, second ed., Prentice-Hall, 1999.
[35] C.Y. Wang, Transport issues in polymer electrolyte fuel cell, in: Purdue Heat Transfer Celebration, 2003.
[36] A. Fischer, J. Jindra, H. Wendt, Porosity and catalyst utilization of thin layer cathodes in air operated PEM-fuel cells, J. Appl. Electrochem. 28 (1998) 277–282.
[37] D. Natarajan, T.V. Nguyen, Three-dimensional effects of liquid water flooding in the cathode of a PEM fuel cell, J. Power Sources 115 (2002) 66–80.